Advanced Structured Materials

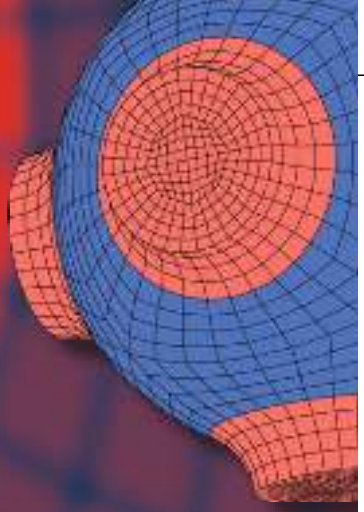

Andreas Öchsner
Holm Altenbach *Editors*

Advances in Bio-Mechanical Systems and Materials

Springer

Advanced Structured Materials

Volume 40

For further volumes:
http://www.springer.com/series/8611

Andreas Öchsner · Holm Altenbach
Editors

Advances in Bio-Mechanical Systems and Materials

Springer

Editors
Andreas Öchsner
Faculty of Biosciences and Medical Engineering (FBME)
University of Technology Malaysia—UTM
Skudai
Malaysia

and

Faculty of Engineering and Built Environment
The University of Newcastle
Newcastle
Australia

Holm Altenbach
Lehrstuhl für Technische Mechanik
Otto-von-Guericke-Universität
Magdeburg
Germany

and

Fakultät für Maschinenbau
Institut für Mechanik
Magdeburg
Germany

ISSN 1869-8433 ISSN 1869-8441 (electronic)
ISBN 978-3-319-00478-5 ISBN 978-3-319-00479-2 (eBook)
DOI 10.1007/978-3-319-00479-2
Springer Cham Heidelberg New York Dordrecht London

Library of Congress Control Number: 2013944881

Printed on acid-free paper

Springer is part of Springer Science+Business Media (www.springer.com)

Preface

The idea of this monograph is to present the latest results related to biomechanical systems and materials. Biomechanical systems within this book are prostheses (lower limb and orbitarian cranial cavity), implants (such as for the femoral bone, microimplants for dental surgery, and total hip replacement), medical operation robots (for tumor removal), and muscular retraining systems (for forearm and wrist). To characterize and design such systems, a multidisciplinary approach is required which involves the classical disciplines of mechanical/materials engineering (design, analysis, and properties), and biology/medicine. The challenge in such an approach is that views, concepts or even languages are sometimes different from discipline to discipline and the interaction and communication of the scientists must be first developed and adjusted. In the context of materials, the interaction of materials with mechanical systems, their description as a mechanical system or their mechanical properties is covered.

The 6th International Conference on Advanced Computational Engineering and Experimenting, ACE-X 2012, was held in Istanbul, Turkey, from 1 to 4 July 2012 with a strong focus on computational-based and supported engineering. This conference served as an excellent platform for the engineering community to meet with each other and to exchange the latest ideas. This volume contains 11 revised and extended research articles written by experienced researchers participating in the conference. The book will offer the state-of-the-art of tremendous advances in biomechanical systems and materials.

The organizers and editors wish to thank all the authors for their participation and cooperation which made this volume possible. Finally, we would like to thank the team of Springer-Verlag, especially Dr. Christoph Baumann, for the excellent cooperation during the preparation of this volume.

May 2013

Andreas Öchsner
Holm Altenbach

Contents

Lesion Eccentricity and Fractional Flow Reserve and Coronary Flow Reserve in Coronary Arteries

Ashkan Javadzadegan, Andy S. C. Yong, Leonard Kritharides and Masud Behnia

Abstract Fractional flow reserve has shown to be a gold standard in assessment of functional significance of coronary artery stenosis. Lesion eccentricity is an important geometric parameter which may affect the translational hemodynamics. Three dimensional quantitative coronary angiography (3D-QCA) was used to reconstruct the proximal or mid left anterior descending artery of 56 patients. The fractional flow reserve (FFR) was measured using pressure–temperature sensor guidewire and the effects of lesion eccentricity (EI) was investigated on the correlation between FFR diameter stenosis (DS), area stenosis (AS), minimum lumen diameter (MLD) and minimum lumen area (MLA). A linear regression analysis showed a non-significant correlation between FFR and DS, AS, MLD and MLA. In order to improve the correlations, a receiver operating characteristic (ROC) curve analysis was used to identify the best cut-off value of eccentricity to predict FFR ≤ 0.75. It was found that for lesions whose eccentricity is above the cut-off, the correlations are significant; however, the correlations are weak for lesions with eccentricity below the cut-off.

Keywords Coronary artery • Eccentricity • Fractional flow reserve • Stenosis

1 Introduction

Coronary angiography has become a gold standard in physiological assessment of coronary artery disease. Accurate determination of the functional significance of lesion severity is important for clinical decision making in epicardial coronary stenoses [1].

A. Javadzadegan · M. Behnia (✉)
Department of Mechanical Engineering, The University of Sydney, Sydney, Australia
e-mail: masud.behnia@sydney.edu.au

A. Javadzadegan
e-mail: ashkan.javadzadegan@sydney.edu.au

A. S. C. Yong · L. Kritharides
Department of Cardiology, Concord Hospital, Sydney, Australia

A. Öchsner and H. Altenbach (eds.), *Advances in Bio-Mechanical Systems and Materials*, Advanced Structured Materials 40, DOI: 10.1007/978-3-319-00479-2_1,

Fractional flow reserve (FFR), available in the catheterization laboratory, is a gold standard to measure the functional significance of coronary stenoses. It is calculated as the distal mean pressure to proximal mean pressure during hyperemia [2]. Previous studies showed that FFR $\leq$ 0.75 is a reliable lesion specific index to distinguish significant stenosis from non significant one [2–4]. Coronary lesion severity is often graded by the amount of lumen encroachment or stenosis it causes, and most clinical decisions are made based on lesion stenosis severity [5]. However, other lesion characteristics such as eccentricity may contribute to the extent of in situ physiological disturbance.

Lesion eccentricity refers to the extent the lumen is displaced from the centre of a vessel [6] and in an anatomical survey of diseased coronary arteries, the majority were found to have eccentric lesions [7]. Lesion eccentricity is an important geometric parameter that should be investigated when assessing the nature of coronary stenoses. Previous studies showed that lesion length and plaque volume are important geometric variables which have significant impacts on the physiological significance of coronary lesions [8, 9]. Most of previous studies have correlated FFR with different 2D and 3D geometric parameters [10–17]. We have recently related FFR to 3D coronary angiography [18]. However, to the best of our knowledge no one has systematically investigated the correlation between lesion eccentricity and FFR.

The aim of this study is to assess the effect of lesion eccentricity (EI) on the correlation between FFR and diameter stenosis (DS), minimum lumen diameter (MLD), minimum lumen area (MLA) and area stenosis (AS).

2 Methods

2.1 Patient Cohort

The study population consisted of 56 consecutive patients who presented to the cardiac catheterization laboratory for elective fractional flow reserve guided coronary intervention of a single target lesion in the proximal or mid left anterior descending artery at our institution were recruited. All patients underwent coronary angiography and physiological measurements within their coronary arteries. Written informed consent was obtained for all patients, and the study was approved by the Human Ethics Committee of Concord Hospital. Three dimensional quantitative coronary angiography (3D-QCA) and fractional flow reserve (FFR) measurements were performed as described [18, 19].

2.2 Two and Three Dimensional Quantitative Coronary Angiography (3D-QCA)

3DRs of 56 patients were obtained using three-dimensional quantitative coronary angiography as previously described [18, 19].

2.3 Fractional Flow Reserve (FFR) and Eccentricity Index (EI) Calculation

FFR measurements was performed as previously published [18, 19]. EI was quantified for each lesion as previously described [6].

2.4 Computational Fluid Dynamics Analysis

CFD analysis was performed using ANSYS CFX (v14.0, ANSYS-Fluent Inc., Lebanon, NH, USA), a finite volume based software. Flow for the simulation was assumed to be 3D, laminar and steady. The walls were considered solid and a zero-velocity, no-slip boundary condition was adopted at the walls. Blood was modelled as an incompressible Newtonian fluid with a dynamic viscosity of 0.0035 Pa.s and a density of 1050 kg/m^3. The inlet and outlet boundary conditions were set for the reconstructed patients' arteries to the measured Pa and Pd.

2.5 Statistical Analysis

Results are expressed as mean $\pm$ standard deviation unless otherwise stated. Normality of the data was determined using the D'Agostino Pearson test and verified using histogram plots. Spearman's correlation was performed for non-parametric data. A linear regression analysis was used to obtain a correlation between 2D and 3D parameters and FFR. The best cut-off value for predicting FFR $\leq$ 0.75 was established by a receiver operating characteristic (ROC) curve analysis. Statistical analyses were performed using GraphPad Prism v. 5.01 (GraphPad Software, La Jolla, California) and SPSS v. 15 (SPSS, Chicago, Illinois). A two-sided P value of < 0.05 is considered significant.

3 Results

3.1 Baseline Clinical and Lesion Characteristics

Baseline clinical and lesion characteristics are shown in Table 1. 73 % of the vessels assessed were the left anterior descending (LAD), 14 % were left circumflex (LCX) and 13 % were right coronary artery (RCA). The best cut-off value for predicting FFR $\leq$ 0.75 was established by a receiver operating characteristic (ROC) curve analysis (sensitivity of 62 %, specificity 56 %). To predict FFR $\leq$ 0.75, the optimal cut-off value for EI were 0.4 (sensitivity of 62 %, specificity 56 %).

Table 1 Demographic, baseline clinical and angiographic characteristics

Variable	All	EI > 0.4	EI ≤ 0.4
Age, mean–yr	61 ± 10	62 ± 9	61 ± 10
LAD	41 (73)	21 (51)	20 (49)
LCX	8 (14)	2 (25)	6 (75)
RCA	7 (13)	1 (15)	6 (85)
Ref. D(mm)	2.63 ± 0.47	2.7 ± 0.51	2.58 ± 0.44
MLD(mm)	1.23 ± 0.43	1.4 ± 0.38	1.09 ± 0.43
EI	0.38 ± 0.22	0.58 ± 0.15	0.22 ± 0.12
%DS	53.5 ± 13	50.9 ± 12.9	55.5 ± 12.7
Mean FFR	0.63 ± 0.18	0.65 ± 0.2	0.62 ± 0.17

Values are mean ± SD. LAD indicates left anterior descending artery
LAD, left anterior descending; *LCX*, left circumflex; *RCA*, right coronary artery
Ref. D, Reference diameter; *MLD*, Minimal lumen diameter

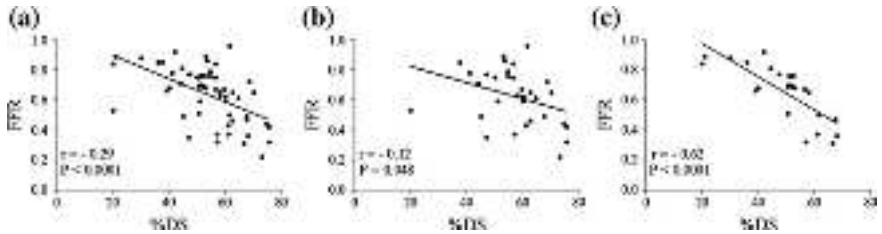

Fig. 1 Relationship between fractional flow reserve (FFR) and coronary diameter stenosis (%DS). **a** All lesions. **b** Lesions with EI ≤ 0.4. **c** Lesions with EI > 0.4

3.2 Effect of Lesion Eccentricity on Correlation Between 2D and 3D Parameters and FFR

According to the eccentricity cut-off value, the lesions were divided into three subgroups, overall cohort of 56 lesions, the lesions with EI > 0.4 and the lesions with EI ≤ 0.4. Linear regression analysis demonstrated a non-significant correlation between FFR and %DS ($r = -0.29$, $P < 0.0001$; Fig. 1a) and also FFR and %AS ($r = -0.37$, $P < 0.0001$; Fig. 2a) for whole cohort of lesions. Separate linear regression analysis revealed that there was a significant improvement in the correlation between FFR, %DS ($r = -0.62$, $P < 0.0001$; Fig. 1c) and %AS ($r = -0.63$, $P < 0.0001$; Fig. 2c) for the lesions with EI > 0.4, as compared to the lesions with EI ≤ 0.4 (%DS: $r = -0.12$, $P = 0.048$; Fig. 1b, %AS: $r = -0.21$, $P = 0.0058$; Fig. 2b).

Comparable improvement was also observed in the correlation between FFR, MLD and MLA for more eccentric lesions (EI > 0.4) (MLD: $r = 0.50$, $P = 0.0001$, MLA: $r = 0.51$, $P = 0.0001$), as compared with more concentric lesions (EI ≤ 0.4) (MLD: $r = 0.08$, $P = 0.11$, MLA: $r = 0.12$, $P = 0.048$) (Table 2).

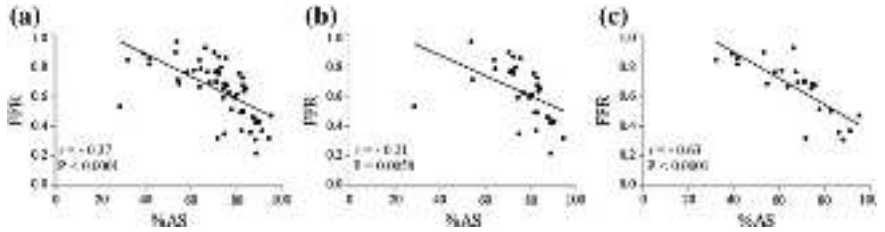

Fig. 2 Relationship between fractional flow reserve (FFR) and coronary area stenosis (%AS). **a** All lesions. **b** Lesions with EI $\leq$ 0.4. **c** Lesions with EI > 0.4

Table 2 Effect of EI on correlation of 3D and 2D parameters with the FFR

Parameter	Whole cohort of lesions	EI $\leq$ 0.4	EI > 0.4
%DS (2D)	r = − 0.29; $P < 0.0001$	r = − 0.12; $P = 0.048$	r = − 0.62; $P < 0.0001$
MLD (2D)	r = 0.23; $P = 0.0001$	r = 0.08; $P = 0.11$	r = 0.50; $P = 0.0001$
MLA (3D)	r = 0.26; $P < 0.0001$	r = 0.12; $P = 0.048$	r = 0.51; $P = 0.0001$
%AS (3D)	r = − 0.37; $P < 0.0001$	r = − 0.21; $P = 0.0058$	r = − 0.63; $P < 0.0001$

4 Discussion

These data demonstrates that for overall cohort of patients, there is a weak correlation between FFR and DS, MLD, MLA and AS. However, by dividing the lesion into two subgroups; lesions with high eccentricity (above EI 0.4) and lesions with less eccentricity (below EI 0.4), the correlations are significantly improved when separate linear regression analysis is performed for each subgroup. This implies that careful evaluation of lesion eccentricity during angiography may improve the identification of functionally significant coronary stenoses.

References

1. Topol, E.J., Nissen, S.E.: Our preoccupation with coronary luminology. The dissociation between clinical and angiographic findings in ischemic heart disease. Circulation **92**, 2333–2342 (1995)
2. Berger, A., et al.: Long-term clinical outcome after fractional flow reserve-guided percutaneous coronary intervention in patients with multivessel disease. J. Am. Coll. Cardiol. **46**, 438–442 (2005)
3. Pijls, N.H., et al.: Percutaneous coronary intervention of functionally nonsignificant stenosis: 5-year follow-up of the DEFER Study. J. Am. Coll. Cardiol. **49**, 2105–2111 (2007)
4. Potvin, J.M., et al.: Usefulness of fractional flow reserve measurements to defer revascularization in patients with stable or unstable angina pectoris, non-ST-elevation and ST-elevation acute myocardial infarction, or atypical chest pain. Am. J. Cardiol. **98**, 289–297 (2006)
5. Shaw, L.J., et al.: Optimal medical therapy with or without percutaneous coronary intervention to reduce ischemic burden: results from the Clinical Outcomes Utilizing Revascularization and Aggressive Drug Evaluation (COURAGE) trial nuclear substudy. Circulation **117**(10), 1283–1291 (2008)

6. Li, F., et al.: The association of lesion eccentricity with plaque morphology and components in the superficial femoral artery: a high-spatial-resolution, multi-contrast weighted CMR study. J. Cardiovasc. Magn. Reson. **12**, 37 (2010)
7. Yamagishi, M., et al.: Morphology of vulnerable coronary plaque: insights from follow-up of patients examined by intravascular ultrasound before an acute coronary syndrome. J. Am. Coll. Cardiol. **35**(1), 106–111 (2000)
8. Brosh, D., et al.: Effect of lesion length on fractional flow reserve in intermediate coronary lesions. Am. Heart J. **150**, 338–343 (2004)
9. Kolozsvari, R., et al.: Plaque volume derived from three-dimensional reconstruction of coronary angiography predicts the fractional flow reserve. Int. J. Cardiol. (2011). doi:10.1016/j.ijcard.2011.04.010
10. Briguori, C., et al.: Intravascular ultrasound criteria for the assessment of the functional significance of intermediate coronary artery stenoses and comparison with fractional flow reserve. Am. J. Cardiol. **87**, 136–141 (2001)
11. Jasti, V., et al.: Correlations between fractional flow reserve and intravascular ultrasound in patients with an ambiguous left main coronary artery stenosis. Circulation **110**, 2831–2836 (2004)
12. Takagi, A., et al.: Clinical potential of intravascular ultrasound for physiological assessment of coronary stenosis: relationship between quantitative ultrasound tomography and pressure-derived fractional flow reserve. Circulation **100**, 250–255 (1999)
13. Tobis, J., et al.: Assessment of intermediate severity coronary lesions in the catheterization laboratory. J. Am. Coll. Cardiol. **49**, 839–848 (2007)
14. Lamm, C., et al.: High-fidelity translesional pressure gradients during percutaneous transluminal coronary angioplasty: correlation with quantitative coronary angiography. Am. Heart J. **126**, 66–75 (1993)
15. Hanekamp, C.E.E., et al.: Comparison of quantitative coronary angiography, intravascular ultrasound, and coronary pressure measurement to assess optimum stent deployment. Circulation **99**, 1015–1021 (1999)
16. Abizaid, A., et al.: Clinical, intravascular ultrasound and quantitative angiographic determinants of the coronary flow reserve before and after percutaneous transluminal coronary angioplasty. Am. J. Cardiol. **82**, 423–428 (1998)
17. Moses, J.W., et al.: Relation between single tomographic intravascular ultrasound image parameters and intracoronary Doppler flow velocity in patients with intermediately severe coronary stenoses. Am. Heart J. **135**, 988–994 (1998)
18. Yong, A.S.C., et al.: Three-dimensional and two-dimensional quantitative coronary angiography, and their prediction of reduced fractional flow reserve. Eur. Heart J. **32**(3), 345–353 (2011)
19. Javadzadegan, et al.: Flow recirculation zone length and shear rate are differentially affected by stenosis severity in human coronary arteries. Am. J. Physiol. Heart Circ. Physiol. **304**, 559–566 (2013)
20. Ng, M.K., et al.: Invasive assessment of the coronary microcirculation: superior reproducibility and less hemodynamic dependence of index of microcirculatory resistance compared with coronary flow reserve. Circulation **113**(17), 2054–2061 (2006)

Design of a Biomechatronics Robot to Provide Therapy and to Remove Tumors

R. Leticia Corral-Bustamante, E. Siqueiros-Loera, J. N. Hernández Magdaleno, J. M. Berlanga-Reyes, H. Mendoza-Olivas, J. Salayandía-Ramos, A. Heiras-Torres and M. A. Anchondo-Cuilty

Abstract This chapter presents the design of a biomechatronics device by means of a prototype that includes mechanical, electronic and computational design with biomedical applications. The robot design was done in SolidWorks 2009, and consists of a Cartesian robot with 3 degrees of freedom (RC3GL), whose pieces were fabricated using advanced manufacturing in a CNC machine.The objective of this design is that the robot is capable of moving in the x, y and z Cartesian axes controlled by a computer. Furthermore, its terminals should serve to perform functions to locate damaged tissue to provide microwave cancer therapy and remove

R. Leticia Corral-Bustamante (✉) · E. Siqueiros-Loera · J. N. H. Magdaleno · J. M. Berlanga-Reyes · H. Mendoza-Olivas · J. Salayandía-Ramos · A. Heiras-Torres · M. A. Anchondo-Cuilty
Department of Industrial and Mechatronics Engineering, Technological Institute of Cuauhtémoc City, Tecnológico Ave. S/N, Z.P. 31500, Cuauhtémoc City, Chihuahua, Mexico
e-mail: leticia.corral@cimav.edu.mx

E. Siqueiros-Loera
e-mail: liz_siqueiros@yahoo.com.mx

J. N. H. Magdaleno
e-mail: josenino2001@hotmail.com

J. M. Berlanga-Reyes
e-mail: martin.berlanga@gmail.com

H. Mendoza-Olivas
e-mail: solotenchita57@hotmail.com

J. Salayandía-Ramos
e-mail: javier.salayandia@imss.gob.mx

A. Heiras-Torres
e-mail: alberto.heiras@gmail.com

M. A. Anchondo-Cuilty
e-mail: ancuma75@hotmail.com

A. Öchsner and H. Altenbach (eds.), *Advances in Bio-Mechanical Systems and Materials*, Advanced Structured Materials 40, DOI: 10.1007/978-3-319-00479-2_2,

tumors, with the purpose of contributing in the design of equipment that serves to make the manual labor that perform an oncologist with patients in Chihuahua, México.

Keywords Robot • Mechanical design • Electronic design • Programming • Heat transfer software • Advanced manufacturing • Therapy • Radiofrequency • Microwaves • Removal • Tumors • Electronic circuits • Bioheat equation

Abbreviations

RC3GL	Cartesian robot with 3 degrees of freedom
RF	radio frequency
LM35	temperature sensor
LCD	screen of liquid crystal

1 Introduction

This chapter is a contribution to the state-of-art-of robotics, which is the branch of technology devoted to the design, construction, operation, structural arrangement, manufacture and application of robots. Robotics combines various disciplines such as: mechanics, electronics, computer science, artificial intelligence and control engineering, among others [1, 2].

The aim of this work is the physical and experimental realization of a mechatronic robot with heat transfer functions [3–9] to remove tumors in therapy and to benefit the health sector.

Previously, a part of the robot (RC3GL, [11]) was designed in the software Solid Works 2009 [10], which were developed through advanced manufacturing in a CNC machine (mechanical design).

Recently, a part of the robot (RC3GL, [11]) was designed in the software Solid Works 2009 [10] and produces through advanced manufacturing in a CNC machine (mechanical design).

The actual focus is on the realization of the entire design: solid works, mechanical, electronic and computational designs to develop a robot that has two parts: (a) RC3GL [11] capable of moving in the three Cartesian axes and, (b) two terminals adapted to RC3GL to conduct cancer therapy in order to remove tissue damaged by microwaves and remove tumors, especially in human organs such as the liver.

In the framework of the computational design, three programming languages of high and intermediate level were used to write the software to control RC3GL: Flash CS5, Visual Basic.NET and Action Script 2.0. These tools were used to develop a power and control circuit to establish communication and to control the movements of the robot.

The results obtained so far in building the robot consists of two parts: (a) the designs: solid works, mechanical, electronic and computational; and (b) modeling and simulation.

Talking about the medical functions that the robot is supposed to perform, it must execute the work of radiosurgery, as the medical procedure of *radiotherapy* is called, where narrow beams of radiation in the megavoltage are administered by multiple convergent and formed fields. This allows having a high dose of irradiation which can be accurately located in an area or specific anatomical structure, avoiding toxic doses to adjacent tissues [12–16].

The terminals are expected to provide therapy to remove damaged tissue tumors, and to perform a precise function through the correct location of the affected tissue area as in radiosurgery. To do this, we modeled and simulated the functions of human tissue with the Comsol Multiphysics software [17–22]. The temperatures are expected to warm the terminals and the damaged tissue where the therapy and/or removal is undergoing, and reach the ideal temperatures to perform the medical tasks.

Despite all the wealth and new technologies in robot developments, there is no Cartesian robot that performs the heat transfer function with applications in oncology [12–16] at present in the market.

The first tests will be conducted with animal tissue during the II/2012 semester, and precision and refinement testing of the functions for which the robot was designed, is expected to be completed in the I/2013 semester with the conclusion of the student`s theses[1] that are working on this project.

The Solid Works design of the pieces of the robot is original, and all parts were machined with nylacero which is a modified copolymer lauryl lactam with greater tensile strength and impact resistance. This type of Cartesian robots tackles a lot of automation tasks such as handling and assembly of parts and performing reliably, quickly and cost-effective of several functions. This offers the enormous potential to use the same robot for various applications, thanks to the modular robotic systems.

The Solid Works 2009 design [10] for the robot without medical terminals has the copyright registration No. 03-2010-012012301500-01 and is entitled: Cartesian robot with three degrees of freedom.[2]

The software was chosen to simulate the mechanical design which is an easily readable model. Furthermore, it allows the simulation and optimization of the parameters using only standard values, such as number of teeth, diametral pitches, materials, among others, and presents results in a graphical and numerical form

[1] Scholarships DGEST: 03 2010-068, 069, 070, 071 and 072 ID of thesis project for: D. J. Camacho Medina, J. Ochoa Morales, O. G. Ochoa González, A. Ruiz Mendoza and D. A. Villalba Caraveo, respectively. Moreover, J. I. Loya Valladares, L. A. Rodríguez Gándara, W. Ceballos Castillo, A. E. Ledezma Lechuga, L. E. Torres González, I. Arias Chávez, D. A. Rodríguez García, M. A. Torres Navarro.

[2] Degree Theses of Emmanuel Núñez Jáquez.

and has substantial improvements over previous versions. Solid Works is a program for 3D mechanical design that uses a graphical environment based on Microsoft Windows, intuitive and easy to handle. The main features that make Solid Works a versatile and accurate tool is its ability to create assemblies from parts, the fact that the parts can be easily modified and uses standard measures in a bidirectional way with all applications. Also it uses the layout manager (Feature Manager) that facilitates the rapid change in three-dimensional operations sketch without having to redo the design already reflected in the rest of their associated documents. Along with the part design tools, assemblies and drawings, SolidWorks [10] includes productivity tools, project management, presentation, analysis and simulation in its mechanical design.

2 Nomenclature

C	tissue's specific heat (J kg^{-1} K^{-1})
C_b	blood's specific heat (J kg^{-1} K^{-1}), 3639 [J kg^{-1} K^{-1}]
C_p	heat capacity at constant pressure for the biological tissue (J kg^{-1} K^{-1}), 3600 [J kg^{-1} K^{-1})]
J^e	externally generated current density (A m^{-2})
P_{av}	time-averaged power flow in the cable
Q_j	current source (A m^{-3})
Q_{met}	heat source from metabolism (W m^{-3})
Q_{ext}	external heat source from spatial heating (W m^{-3})
r_{inner}	dielectric's inner radii (m)
r_{outer}	dielectric's outer radii (m)
t	temporal coordinate (s)
T	temperature (°C or K)
T_b	arterial blood temperature (°C), 37 [°C]
V	potential
z	cylindrical coordinate centered on the axis of the coaxial cable
Z	wave impedance in the dielectric of the cable

Greek letters

δ_{ts}	time-scaling coefficient
ε	relative permittivity
κ	thermal conductivity (W m^{-1} K^{-1})
λ	wavelength in the medium (m)
φ	cylindrical coordinate centered on the axis of the coaxial cable
ρ	tissue density (kg m^{-3})
ρ_b	blood's density (kg m^{-3}), 1,000 [kg m^{-3}]
σ	electric conductivity (S m^{-1})
ω	angular frequency
ω_b	perfusion rate (1/s), 0.0036 [s^{-1}]

3 Modeling

Modeling of the robot functions was performed by the Comsol Multiphysics software [17–22], which makes use of the heat transfer capacity [3–9] to simulate therapy and the removal of damaged tissue cells. The human tissue is modeled as a cylindrical geometry to which a conductive heat is applied to burn the cancer cells. The module of heat transfer in biological tissues uses the bioheat transfer interface of Comsol and plays an important role in technology for medical purposes. Comsol uses the approximation of Penne [4] to represent the heat sources from metabolism and blood perfusion. The equation for heat transfer by conduction with this approach is

$$\rho C_p \frac{\partial T}{\partial t} + \nabla \cdot (-\kappa \nabla T) = \rho_b C_b \omega_b (T_b - T) + Q_{met} \tag{1a}$$

The terms on the left-hand side of Eq. (1a) belong to the model of biological tissue, while the terms on theright-hand side provide; provide the bioheat model [3].

Tumor ablation involves passing of four electrodes at a given temperature through the affected tissue. The method involves inserting a tube in which electrical current flows through four electrodes leaving a plunger, to the well localized cancerous tissue. Radio frequencies are used to heat these electrodes due to heat transfer [3–9] up to a temperature between 45 and 50 °C in the tissue. This method serves to increase the cell temperature above 45–50 °C, resulting in protein denaturation with coagulation that is the ultimate cause of cell death and tissue necrosis. RF tumor ablation could be implemented in patients with liver tumors [23, 24], kidney, lung [25], prostate and breast, among others. Currently, a radiation oncologist [12–16, 25] performs this function by hand as far as information is available in the State of Chihuahua.

The probe is a needle (main bar) and four electrode arms as shown in Fig. 1. The needle is electrically isolated, except near the electrode arms. An electric current through the probe creates an electric field in the tissue. The field is the strongest in the immediate vicinity of the probe and generates resistive heating, which dominates around the arms of the probe electrode due to the strong electric field.

This model uses the bioheat equation and the continuous current mode to implement a transient analysis

$$\delta_{ts} \rho C \frac{\partial T}{\partial t} + \nabla \cdot (-\kappa \nabla T) = \rho_b C_b \omega_b (T_b - T) + Q_{met} + Q_{ext} \tag{1b}$$

where,

$$\nabla = \hat{\rho} \frac{\partial}{\partial t} + \frac{\hat{\phi}}{\rho} \frac{\partial}{\partial \phi} + \hat{z} \frac{\partial}{\partial z}$$

and,

$$-\nabla \cdot \left(\sigma \nabla V - \mathbf{J}^e\right) = Q_j \overset{\mathbf{J}^e = Q_j = 0}{\longrightarrow} -\nabla \cdot (\sigma \nabla V) = 0 \tag{2}$$

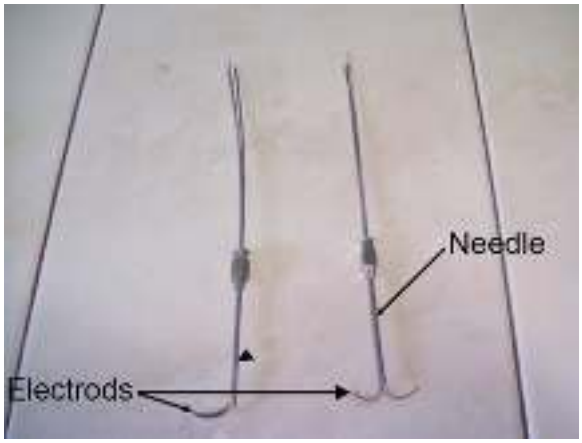

Fig. 1 Electrodes inserted into a needle to remove tumors

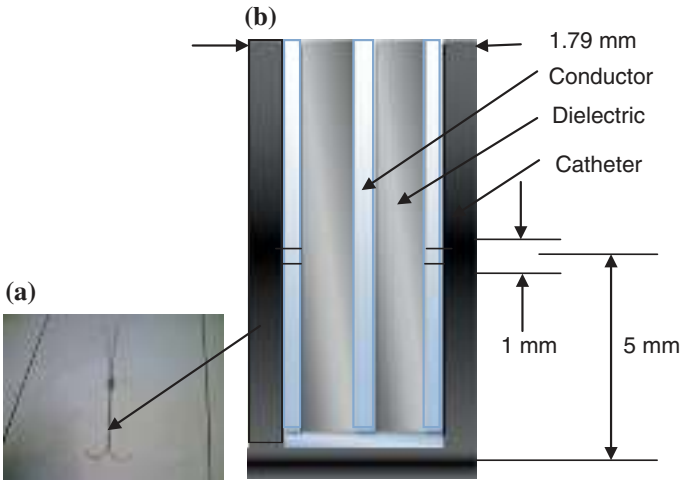

Fig. 2 Antenna geometry for microwave coagulation therapy. **a** A coaxial cable with a ring-shaped slot cut in the outer conductor which produces a short circuit at the tip. **b** A plastic catheter surrounding the antenna

It is assumed in the computational model that the body tissue is a cylinder and its temperature remains at 37 °C during the entire process. The model locates the probe along the centerline of the tissue such that its electrodes cross the region where the tumor is located.

The terminal to perform the cancer therapy by microwave consists of the following elements (see Fig. 2a): an instrument that converts electrical energy to electromagnetic energy by a coaxial antenna that emits a microwave.

The main instrument is a physical device that carries electrical energy to a very small antenna which emits microwaves onto a piece of human tissue.

The top of the antenna with a load of 128–1,300 milli volts is introduced to the center of the tumor, emitting microwaves, creating friction in the tissue of the molecules, generating heat transfer (electromagnetic field modeled by Eq. (1a, b) to a temperature of 50 °C to kill cancer cells.

The innovation that is intended to provide is to control three fundamental aspects: the induced voltage and time per session controlled by microcontrollers and temperature in order to achieve a good therapy.

The modeling of the microwave cancer therapy is done in two-dimensions with cylindrical coordinates as the problem is of rotational symmetry (see Fig. 2b).

An electromagnetic wave propagating in a coaxial cable is characterized by transverse electromagnetic fields (TEM). Assuming harmonic time fields with complex amplitudes containing the phase information, the appropriate equations are:

$$\mathbf{E} = \mathbf{e}_r \frac{C}{R} e^{j(\omega t - \kappa z)} \tag{3}$$

$$\mathbf{H} = \mathbf{e}_\varphi \frac{C}{Z} e^{j(\omega t - \kappa z)} \tag{4}$$

$$\mathbf{P}_{av} = \int_{r_{inner}}^{r_{outer}} \mathrm{Re}\left(\frac{1}{2}\mathbf{E} \times \mathbf{H}^*\right) 2\pi r dr = \mathbf{e}_z \frac{C^2}{Z} \ln\left(\frac{r_{outer}}{r_{inner}}\right) \tag{5}$$

The propagation constant κ is related to the wavelength in the medium λ as

$$\kappa = \frac{2\pi}{\lambda} \tag{6}$$

In tissue, the finite axial component of the electric field, and the azimuthal component of the magnetic field allow to model the antenna to a transverse magnetic axial symmetry (TM) and the wave equation becomes scalar $\mathbf{H}_\varphi$ as in

$$\nabla \times \left(\left(\varepsilon_r - \frac{j\sigma}{\omega\varepsilon_0}\right)^{-1} \nabla \times \mathbf{H}_\phi\right) - \mu_r \kappa_0^2 \mathbf{H}_\phi = 0 \tag{7}$$

The boundary conditions on the metal surfaces are

$$\mathbf{n} \times \mathbf{E} = 0 \tag{8}$$

The feed point is modeled with a boundary condition of a source with 10 W. This is a reflection boundary condition of first order with an input field $\mathbf{H}_{\varphi 0}$

$$\mathbf{n} \times \sqrt{\varepsilon}\mathbf{E} - \sqrt{\mu}\mathbf{H}_\phi = -2\sqrt{\mu}\mathbf{H}_{\phi 0} \tag{9}$$

$$\mathbf{H}_{\phi 0} = \frac{\sqrt{\frac{\mathbf{P}_{av} Z}{\pi r \ln\left(\frac{r_{outer}}{r_{inner}}\right)}}}{r} \tag{10}$$

to an input power of W $\mathbf{P}_{\text{av}}$ as shown in the average power flow in time. The antenna radiates in the tissue where a damped wave propagates: (1) an absorption boundary condition at some distance from the antenna, without excitement, in all the external borders, and (2) A symmetry boundary condition at the boundaries $r = 0$, namely

$$E_r = 0 \tag{11}$$

$$\frac{\partial E_z}{\partial r} = 0 \tag{12}$$

The domain and boundary equations of heat transfer are satisfied by the bioheat equation which describes this phenomenon in steady state as

$$\nabla \cdot (-\kappa \nabla T) = \rho_b C_b \omega_b (T_b - T) + Q_{met} + Q_{ext} \tag{13}$$

$$Q_{met} = 0 \tag{14}$$

$$Q_{ext} = \frac{1}{2}\text{Re}\left[(\sigma - j\omega\varepsilon)\,\mathbf{E} \cdot \mathbf{E}^*\right] \tag{15}$$

The model assumes that the rate of perfusion of blood is $\omega b = 0.0036\ s^{-1}$, and that the blood enters the liver at a body temperature of $T_b = (37 + 273.15)$ K and is heated up to a temperature T. The heat capacity of the blood is $C_b = 3{,}639$ J/kg K. These data are used to model the heat transfer only in the domain of the liver. Where this field is truncated, the insulation is used, namely:

$$\mathbf{n} \cdot \nabla T = 0 \tag{16}$$

4 Results and Discussion

This section presents the results of this work by Figs. 3, 4, 5, 6, 7, 8 and 9. Figure 3 a shows the parts that make up the prototype which were developed through advanced manufacturing in a CNC machine, (b) the CNC machine and (c) the Solid Works design of RC3GL.

This robot designed in 2009 by Solid Works [10, 11] is able of moving in three axes, driven by motors of five steps that are managed through a USB port of a computer, with the use of microcontrollers (PIC 18F4550 and PIC16F84A) so that it can be positioned accurately in a Cartesian space. The movement in two axes is assisted by bands, while the other axis is driven with the aid of nuts and bolts [11].

The results of the electronic design were based on a previous analysis that was done on the shape memory material to construct the electrodes of the end piece that must be adapted to RC3GL in order to remove tumors.

The heat transfer behavior of the shape memory materials was studied in order to know in which way the high frequency waves must flow through the material (see Fig. 4).

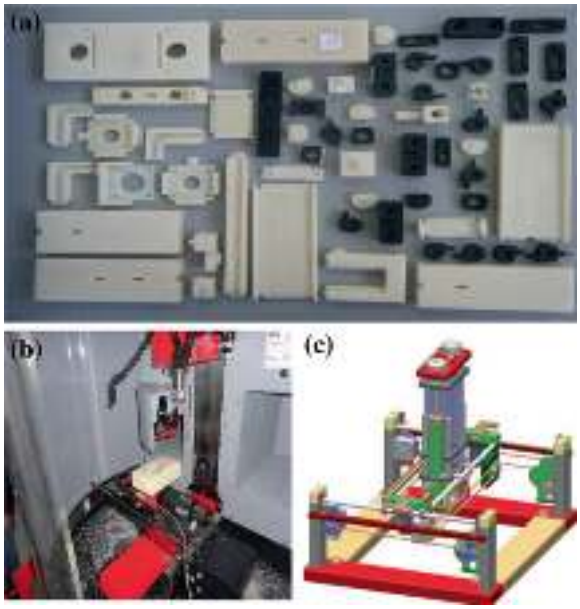

Fig. 3 **a** Some parts of RC3GL were made with advanced manufacturing in a **b** CNC machine. **c** Solid Works design of RC3GL

Based on another study [26] on the thermo mechanical characterization of the *Ni–Ti* alloy to change its original shape by applying heat to the electrodes prior to its yield point, a circuit was developed to induce high frequency electrical waves in the electrodes, that would not risk the the recovery of the material. Furthermore, the process of shape change (reshaping) of the *Nitinol* was studied.

Finally, the terminal was developed in order to remove tumors with four electrodes of *Nitinol* with the required shape memory effect and a search was performed ti find a way to insert the electrodes in liver tissue (Figs. 1 and 2a).

To prevent the electrodes to lose their shape and to penetrate liver tissue removing the tumor, a circuit for controlling the temperature with a 16F873A microcontroller and a temperature sensor LM35 was designed.

A value is assigned to the maximum and minimum temperature and the emission of a pulse to the main circuit obtained, showing the temperature on LCD display (see Fig. 4a).

Figure 4b–e show the circuit board, the soldier components, the full box, the terminals and box components. The electronic design is controlled by an electronic circuit that transmits and receives signals such as radiofrequencies, with buttons, displays, LCDs, indicators, etc. The results are obtained as described below.

A block diagram of the complete circuit for electronically controlling the function of the terminals of the robot is shown in Fig. 5, whose design has been finalized by:

1. Power supply: (a) Voltage source of 5 V and 30 V. (b) Physical voltage source. For the treatment of tumor removal, which is based on the emission of RF through titanium-nickel electrodes, which are introduced into damaged tissue, the RF causes the tumor to be heated and to be burned.

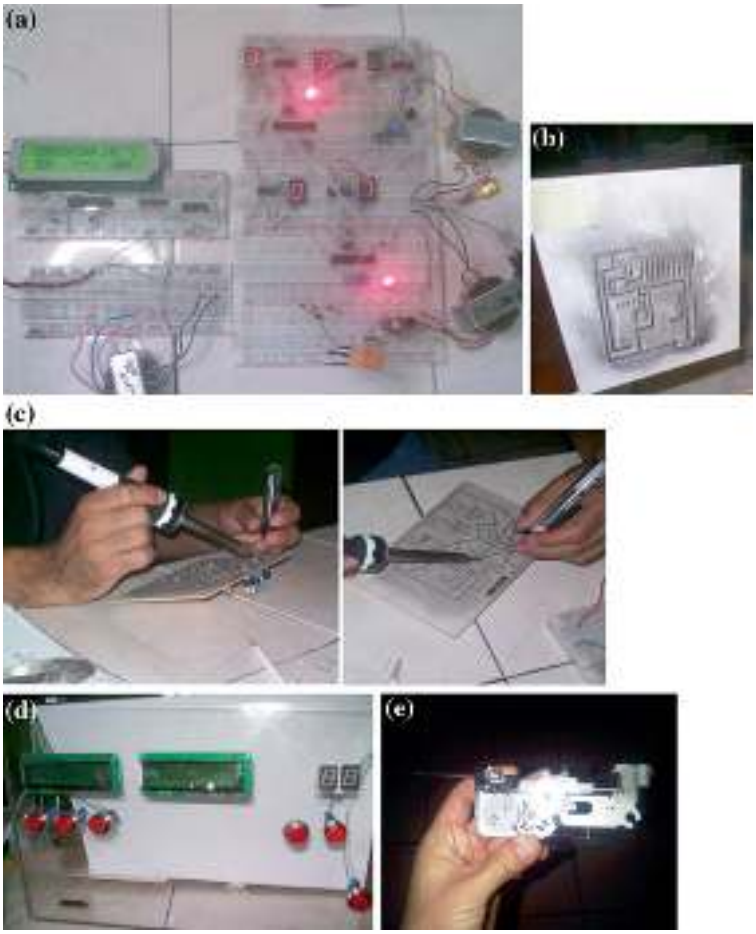

Fig. 4 Electronic design and analysis of shape memory material: (**a**) the temperature controller circuit, (**b**) printed circuit board, (**c**) soldier components, (**d**) full box (Push button, indicators, LCD displays, switch and connection to electrodes) and (**e**) terminals and box components (terminal stripping of liver tumors: shortest amount of time and high accuracy to improve security of the process)

2. Control circuit.

Receives signals from the majority of the circuits.

Controls output to the electrodes.

Gives way to the RF to the electrodes when the start button is pressed and it does not emit this signal when the device is not operating or when the process ends. This signal is received from the timing circuit.

Receive signals from the circuit of the electrode to maintain its temperature at 55 and 65 °C.

Control the input and output or the electrodes on the needle.

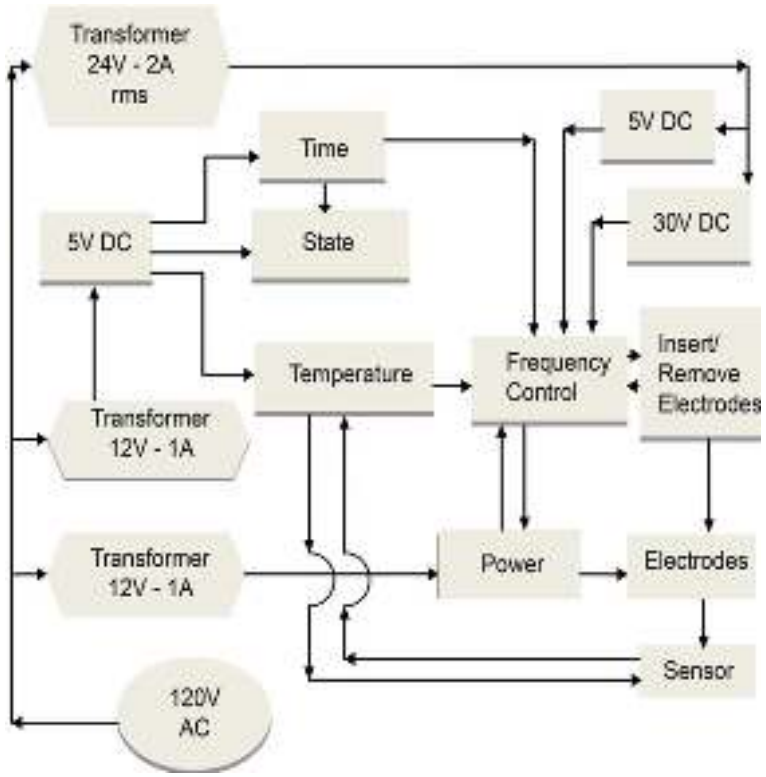

Fig. 5 Block diagram of the complete circuit for electronically controlling the function of the terminals of the robot

3. The frequency-control blocks (Fig. 6). The circuit function is to emit a radio frequency (RF) of 8 MHz with amplitude of about 7 Vpp taking 12.5 V as the basis around this voltage is the oscillation from 9.5 to 15.5 V. It is connected to the electrodes. It is powered by the 24 V supply to 2 A, and converted to direct current. The output goes to the power circuit.

4. Adaptation of the microcontroller to the physical prototype.

The machine has a temperature sensor (LM35) in the electrodes. Range: 55–65 °C.

The sensor sends its signal to the PIC16F873A, this interprets the signal and sends it to an LCD screen which displays the temperature value by sending a signal to the control circuit.

5. Electronic design. Figure 7 shows (a) Physical circuit of temperature, (b) Timing circuit (PIC16F873A), (c) Process State circuit (d) all of the breadboard circuit (LCD screens, displays of the timing circuit, the frequency—control circuit, power supplies, indicators, and all circuits).

6. Circuit for measuring the electrode temperature and to set the time of the process.